Research Square

Preprints are preliminary reports that have not undergone peer review.
They should not be considered conclusive, used to inform clinical practice,
or referenced by the media as validated information.

Kinetics of thermal degradation of Chenopodium Album Stalks

H. A. Abousedera

hoda.abouzied.d@eng-st.cu.edu.eg

Cairo University

M. F. Abadir

Cairo University

M. A. Elmessiery

Cairo University

M. A. Sorour

The Food Technology Research Institute

A. S. Khedr

Cairo University

Article

Keywords: Chenopodium album, Thermal analysis, Kinetics, Alternative fuel

Posted Date: November 17th, 2026

DOI: https://doi.org/10.21203/rs.3.rs-11381014/v1

License: This work is licensed under a Creative Commons Attribution 4.0 International License.
Read Full License

Additional Declarations: No competing interests reported.

Kinetics of thermal degradation of *Chenopodium Album* Stalks

H. A. Abousedera[1], M. F. Abadir[1], M. A. Elmessiery[1], M. A. Sorour[2], and A. S. Khedr[1]

H. A. Abousedera: hoda.abouzied.d@eng-st.cu.edu.eg

M. F. Abadir: magdi.abadir@eng.cu.edu.eg

M. A. Elmessiery: messiery@eng.cu.edu.eg

M. A. Sorour: manar.sorour@arc.sci.eg

A. S. Khedr: abirsafwat@eng.cu.edu.eg

[1] The Chemical Engineering Department, Faculty of Engineering, Cairo University, Giza, Cairo

[2] The Food Technology Research Institute, Giza, Cairo.

Keywords: Chenopodium album – Thermal analysis – Kinetics – Alternative fuel

Abstract

This work explores the kinetics of combustion of a noxious herbaceous biomass, *Chenopodium album* for possible use as alternative fuel. Stalks were cut and sieved to about 4 mm size, then tested for CHNS content, proximate analysis and lignocellulosic content. FTIR disclosed the functional groups contained. Thermal analysis was carried out in air at four heating rates (5, 10, 15 and 20 $K.min^{-1}$) whereby two degradation steps appeared leaving an ash residue of 9-10% at about 600ºC. Kinetic analyses were conducted using two model-methods: Coats-Redfern and Criado's master plots and three iso-conversional methods: FWO, KAS and Friedman's. The first degradation step proved to follow an F1 mechanism and the average values of activation energy, as determined by the three iso-conversional techniques, ranged from 103.88 to 112.31 $kJ.mol^{-1}$. Corresponding values of $\ln A$ were calculated using the kinetic compensation principle. The mechanism of the second degradation step showed a transition from F1 to F2 following increased conversion, with mean values of activation energy ranging from 133.76 to 141.15 $kJ.mol^{-1}$. The possibility of substituting a fossil fuel, charcoal, by *Chenopodium album* stalks, from a sustainability viewpoint was also considered.

1. Introduction

In the last three decades, a global trend has emerged to use agricultural waste as alternative fuels. This process not only preserves natural fossil fuels but also represents a safe disposal of these wastes as a sustainable alternative of open burning which is commonly used and considered a source of air and water pollution [1]. Several conditions must be met to use any agricultural waste as alternative fuel: High calorific value (Above 12000 $kJ.kg^{-1}$), low moisture content, low ash content and resistance to crumbling on transportation [2]. In some industries, like cement making, some other restrictions must be met regarding chemical composition of the waste [3, 4]. Another advantage of using agricultural waste as alternative fuel is the decrease in greenhouse gases emissions [5, 6].

The study of the kinetics of degradation of agricultural wastes, for use as alternative fuel, serves several purposes: The determination of kinetic parameters, such as activation energy indicates the rate at which the biomass decomposes. Also, the decomposition of the waste takes place over several stages taking place at specific temperatures. Determining these temperatures allows for controlling the feeding rate of the waste fuel to maximize exothermic energy released. On the other hand, data from thermal analysis can be used in setting up mathematical models for the design of the reactor using alternative fuel [7, 8]. In general, the sequence of degradation of agricultural waste, whether in air or in an inert atmosphere, starts by the decomposition of hemicellulose and cellulose, followed by the decomposition of lignin [9]. The literature contains a large collection of research work related to the kinetics of decomposition of agricultural waste. In particular, citrus plants waste received a great deal of interest in the works of Lopez-Velasquez et al [9], Chilla et al [10], Mousa et al [11], Muhammad et al [12] and Ismail et al [13]. Most of these authors used non-model iso-conversional models in their work, such as the Flynn-Wall-Ozawa and the Kissinger-Akahira-Sunoze models. When the model method of Coats-Redfern was used, a first order reaction usually characterized the degradation steps. The values of activation energy obtained covered a wide range, starting from 28 to 90 kJ.mol^{-1}[10] to reach 64 to 309 kJ mol^{-1} [13], depending on the conversion level.

Other researchers investigated fruit waste degradation kinetics included pomegranate peels [14] whose average values of calculated activation energy varied from 137.8 to 164 kJ.mol^{-1}, depending on the model used. These values were contradicted by the results of Zaman et al [15] who obtained close values of E, in the range 80.4 to 85.2 by three different methods. Also, pyrolysis kinetics of banana peels were studied by Kumar et al [16] by applying five different techniques, yielding E-values ranging from 108.4 to 201 kJ.mol^{-1}. On the other hand, the kinetics of pyrolysis of date seeds have recently been investigated by Felobes et al [17] who found two steps of degradation whose activation energies averaging 115 and 128 kJ.mol^{-1}. In their work, Xie et al [18] using three heating rates and, applying Coats-Redfern and Horowitz-Metzger method, researched the kinetics of pyrolysis of lignin derived from corncob and peanut shells. They proved that degradation was governed by an Avrami–Erofeev mechanism with $n = 1.5$.

Non-edible plant waste, on the other hand, received their share of studies: Shi et al [19] studied the kinetics of degradation of fallen leaves in nitrogen atmosphere. They used the FWO and KAS iso-conversional techniques to evaluate the kinetic parameters, obtaining close results for activation energy in the range 112.14 to 172.83 kJ.mol^{-1}, depending on the level of conversion. Ten types of edible and non-edible agricultural wastes were investigated by Melikoglu et al [20] who deduced that activation energy values for the whole process of degradation of agricultural wastes lie in the range of 17.8 to 89.3 kJ.mol^{-1}. A study was performed by Lalymia et al [21] on the pyrolysis of stalks of *Agave americana* by considering three different stages of degradation the activation energy of

which averaged 69.18, 87 and 86.85 kJ.mol^{-1}. Three steps of degradation of hyacinth were similarly reported by Abdel-Raouf et al [22] although the kinetics of two steps only were revealed, the average E-values for these steps being 66.19 and 62.02 kJ.mol^{-1}. Similarly, two steps of degradation were obtained by Aly et al on studying the kinetics of pyrolysis of neem seeds [23] using iso-conversional techniques. The reported average values of E for the two steps were considerably close (about 120 kJ.mol^{-1}). Finally, it is worth mentioning that in several cases, degradation of agricultural waste has been reported as being a first order reaction [24, 25].

In the present paper, the thermal degradation, in air, of the herbaceous biomass, *Chenopodium album* (CA) is considered. This weed is globally spread in Africa, Asia, Europe, Australia, North and South America in abundant quantities. Although its leaves and seeds are generally edible, its presence is generally a nuisance because of reported cases of human and cattle poisoning [26, 27] besides being a competitive weed, depriving the original cultivar from its nutrients [28, 29]. In Egypt, its presence causes a serious reduction in wheat yield as it competes for water and soil nutrients, besides being herbicide resistant [30]. One of the main methods to ride any cultivated land from its presence is to uproot its weeds manually. The uprooted weeds are then piled and are usually burnt *in situ*. *Chenopodium album* is a fast- growing plant which can reach up to 2 m in height. (Figure 1) and its stalks have been chosen by the authors to investigate the conditions of its thermal degradation for use as alternative fuel in industrial furnaces. To the authors' knowledge, no previous research has been published to that aim, the closest being the thermal analysis of a parent plant (*Chenopodium quinoa*), in which the authors studied the properties of the plant, including its thermal degradation behavior but did not deal with any kinetic calculations [31].

2. Materials and Experimental

2.1 Characterization

Stalks of *Chenopodium album L.* were collected in August 2025 from a farm in Al Fayoum Governorate, Egypt. The plants were collected by the owner of the farm and supplied to the authors with the owner's permission. The species was identified by Prof. Dr. Manal Sorour, Food Engineering and Packaging Department, Food Technology Research Institute, Agricultural Research Center, Giza, Egypt. *Chenopodium* album is a widespread agricultural weed and is not listed in the Appendices of the Convention on International Trade in Endangered Species of Wild Fauna and Flora [32] [33]. It has not been assessed as threatened on the IUCN Red List. Collection was limited to plants being removed as weeds on the owner's farm and complied with relevant institutional and national guidelines, including the considerations in the IUCN Policy Statement on Research Involving Species at Risk of Extinction.

The main material of interest used consists of the stalks of *Chenopodium album* (CA) (Figure 1) that were cut into small fragments and sieved over sieves 4 and 6 (4.75 and 3.35 mm, respectively), keeping the material retained between the two sieves. After drying in a laboratory oven overnight at 90°C, these were tested for lignocellulosic components content using the methods proposed by Dampanaboina et al [34] and Sura-Kalixto et al [35].

The percentages of carbon, hydrogen, sulfur and nitrogen were determined by CHNS analysis using a FlashSmart Fisher elemental analyzer.

Proximate analysis was carried out to determine moisture content of stalks particulates, following ASTM E1756 [36], ash content (ASTM E1755 [37]) and volatile matter (ASTM E872 [38]). The percentage fixed carbon is calculated by subtracting the previous percentages from 100%. All analyses were duplicated and negligible errors resulted in reporting mean values only.

FTIR of stalks was established using a Bruker ALPHA II Compact FTIR Spectrometer.

The calorific values of raw stalks and the resulting biochar were assessed using a Parr™ Model 6200 Isoperibol Calorimeter

Thermogravimetric analysis (TG – DTG – DSC) was conducted in a thermal analyzer (SDT650) where about 20 mg of material was subjected each time to heating in air, whereby TG and DTG charts were obtained together with the corresponding spreadsheets on which calculations were based. The heating rates used were 5, 10, 15 and 20 $K.min^{-1}$. Each run was duplicated without noticing any perceptible difference in results.

2.2 Kinetic analysis

Kinetic calculations were carried out by first determining the initial and final temperatures of each step of degradation and, knowing the mass of material present at any temperature throughout the step, calculating conversion from the definition:

$$\alpha = \frac{m_0 - m}{m_0 - m_f} \quad (1)$$

Where: m_0 is the initial mass

m is the mass at any temperature throughout the step.

m_f is the final mass at the end of the degradation step.



Figure 1: *Chenopodium album* (CA) plant

The rate of reaction is defined by the expression:

$$\frac{d\alpha}{dt} = k.f(\alpha) \quad (2)$$

The reaction rate constant k is obtained from the Arrhenius equation, so that equation (2) takes the form:

$$\frac{d\alpha}{dt} = Ae^{-\frac{E}{RT}}.f(\alpha) \quad (3)$$

Here, $f(\alpha)$ is the differential kinetic function that depends on the mechanism of reaction. The different forms of that function have been compiled by Khawam et al [39].

If β is the rate of heating (K.min^{-1}), then the previous equation can be written in the form:

$$\frac{d\alpha}{dT} = \frac{A}{\beta}e^{-\frac{E}{RT}}.f(\alpha) \quad (4)$$

This equation can be integrated to give:

$$g(\alpha) = \int \frac{d\alpha}{f(\alpha)} = \frac{A}{\beta}\int e^{-\frac{E}{RT}}.dT \quad (5)$$

The function $g(\alpha)$ is the integral kinetic function, the forms of which are also included in the compilation carried out by Khawam et al [39]. Table 1 reveals the different kinetic mechanisms together with their corresponding kinetic functions.

Table 1: Kinetic functions [39]

Code	Controlling step	$f(\alpha)$	$g(\alpha)$
A	Crystallization and grain growth (Avrami-Erofeev)	$2(1-\alpha).[\ln(1-\alpha)]^{\frac{m-1}{m}}$	$[-\ln(1-\alpha)]^{\frac{1}{m}}$
F0	Zero order reaction	0	α
F1	First order reaction	$1-\alpha$	$-\ln(1-\alpha)$
Fn	nth order reaction $(n \neq 1)$	$(1-\alpha)^n$	$\frac{(1-\alpha)^{1-n}}{1-n}$
R2	Cylindrical: reaction at the interface (Shrinking cylinder)	$2(1-\alpha)^{\frac{1}{2}}$	$1-(1-\alpha)^{\frac{1}{2}}$
R3	Spherical: Surface reaction at the interface (Shrinking sphere)	$3(1-\alpha)^{\frac{2}{3}}$	$1-(1-\alpha)^{\frac{1}{3}}$
D1	One-dimensional diffusion	$1/2\alpha$	α^2
D2	Two-dimensional diffusion	$-\ln(1-\alpha)$	$\alpha+(1-\alpha).\ln(1-\alpha)$
D3	Three-dimensional diffusion (Thin ash layer – Jander equation)	$\frac{3(1-\alpha)^{\frac{2}{3}}}{2-(1-\alpha)^{\frac{1}{2}}}$	$[1-(1-\alpha)^{\frac{1}{3}}]^2$
D4	Spherical: diffusion through ash (Ginstling – Brounstein equation)	$\frac{1}{2[(1-\alpha)^{\frac{-1}{3}}-1]}$	$1-\frac{2}{3}\alpha-(1-\alpha)^{2/3}$

The kinetic parameters of a reaction that determine its rate are the activation energy (E) and the pre-exponential factor (A) or its logarithm. To that aim, model and non-model methods are available. In both methods, either the differential or the integral approach is employed, the former making use of Equation (3), while the latter uses Equation (5).

One of the most used model methods is the integral Coats-Redfern method [39] where an approximation of the integral in Equation (6) results in the following expression:

$$\ln\frac{g(\alpha)}{T_\alpha^2}=\ln\left(\frac{A.R}{\beta.E}\right)-\frac{E}{RT} \qquad (6)$$

Where, β is the heating rate (K.min^{-1}) and R the general gas constant.

Different forms of $g(\alpha)$ are then substituted in the LHS of the equation and plots of $\ln\frac{g(\alpha)}{T_\alpha^2}$ against $1/T$ performed. The straight lines with the highest determination coefficient correspond to the most probable form of $g(\alpha)$. Thereby disclosing the probable reaction mechanism.

Another way of determining the mechanism is to draw Criado's Master Plots [40]. This method, however, requires determining the rate of reaction $\frac{d\alpha}{dt}$ at each conversion level, for a chosen heating rate. Then the two following expressions are determined:

$$\frac{f(\alpha).g(\alpha)}{f(0.5).g(0.5)} \text{ and } \frac{T_\alpha^2}{T_{0.5}^2} \times \frac{\left(\frac{d\alpha}{dt}\right)_\alpha}{\left(\frac{d\alpha}{dt}\right)_{0.5}}$$

The second expression is obtained from experimental DTG data and temperatures corresponding to each conversion level. On the other hand, the first expression is determined for all kinetic functions appearing in Table 1. These two expressions are plotted against conversion and the curve corresponding to the most probable mechanism is the closest to the experimental plot.

The most common non-model methods are iso-conversional methods such as Flynn – Wall – Ozawa (FWO), Kissinger – Akahira – Sunoze (KAS) and Friedman methods. The first two models make use of Equation (5) after performing the integration of $e^{-\frac{E}{RT}}$ using approximations of the expansion of this term as infinite series [41], while the third is a differential method where Equation (2) is directly applied.

In the FWO method, the following expression was deduced [42]:

$$\log\beta = \log\frac{A.E}{R.g(\alpha)} - 0.4567.\frac{E}{RT} \quad (7)$$

Therefore, a plot of $\log\beta$ vs $\frac{1}{T}$ should yield straight lines, for different values of conversion, the slopes of which = $-0.4567\frac{E}{R}$

Also, the KAS method produces an equation in the form [43]:

$$\ln\frac{\beta}{T^2} = \ln\frac{A.R}{E.g(\alpha)} - \frac{E}{RT} \quad (8)$$

This equation reveals that linear plots can be obtained for $\ln\frac{\beta}{T^2}$ against $1/T$, of slope $-\frac{E}{R}$

Friedman method, on the other hand, consists of applying equation (4) in its logarithmic form [45]:

$$\ln\beta\ \frac{d\alpha}{dT} = \ln A.f(\alpha) - \frac{E}{RT} \quad (9)$$

It is common to substitute $\frac{\Delta\alpha}{\Delta T}$ for $\frac{d\alpha}{dT}$, taking $\Delta\alpha = 0.05$. Plots of $\ln\beta\ \frac{\Delta\alpha}{\Delta T}$ against 1/T result in a series of straight lines of slope = $-\frac{E}{R}$.

While these three methods can predict the values of E at each conversion percentage, the logarithm of the pre-exponential factor $(\ln A)$ is obtained using the kinetic compensation mechanism, which has been explained in detail by Vyazovkin et al [46].

This mechanism requires the presence of a linear relation between $\ln A$ and E in the form:

$$\ln A = a + b.E \quad (10)$$

To that aim, values of E are determined using a model-type technique for all mechanisms appearing in Table 1, at any chosen heating rate. Then the values of $\ln A$ are calculated at each temperature from the logarithmic expression of Equation (4):

$$\ln\beta\frac{d\alpha}{dt} = \ln A + \ln f(\alpha) - \frac{E}{RT} \quad (11)$$

The values of the LHS can be obtained from DTG data or by differentiating the equations of conversion – temperature curves

This way, average values of $\ln A$ can be plotted against E, for all reaction mechanisms and the constants a and b in Equation (10) obtained. If now an average value of E, determined by a non-model method is known (E_0), the corresponding mean value of $\ln A_0$ can be calculated by substituting in Equation (10).

3. Results and discussion

3.1 Characteristics of plant stalk

Table 2 details the ultimate, proximate and fiber analyses of stalks.

Table 2: CA Stalk characteristics

Ultimate Analysis		Proximate Analysis		Fiber Analysis	
Element	**Weight%**		**Weight%**		**Weight%**
C	40.58	Moisture	8.3	Cellulose	34.26
H	6.131	Volatile Matter	82.36	Hemi-Cellulose	9.44
N	3.45	Ash	7.3	Lignin	11.99
S	0.607	Fixed Carbon	3.04	Other*	44.4
O	49.232	Gross Calorific Value (kJ/kg)		14994	

* These include extractives, proteins, pectin, ash and inorganic compounds.

In that table, the percentage oxygen, fixed carbon and non-lignocellulosic material were obtained so as each weight% column sum up to 100%. It is worth noticing that the negligible percentage of sulfur present guarantees low SO_x emissions when the waste is used as fuel. As for NO_x emissions, these are mainly due to the nitrogen present in combustion air, so that the level of N in stalks is unlikely to be of any harm.

3.2 FTIR Results

Prior to FTIR analysis, plant stalk fragments were subjected to washing in warm water at 50°C for 4 hours to remove any clinging impurities. The FTIR pattern of the dried stalks showed up as in Figure 2. Characteristic functional groups for the main peaks are shown in Table 3, as obtained from an online data compilation [47].

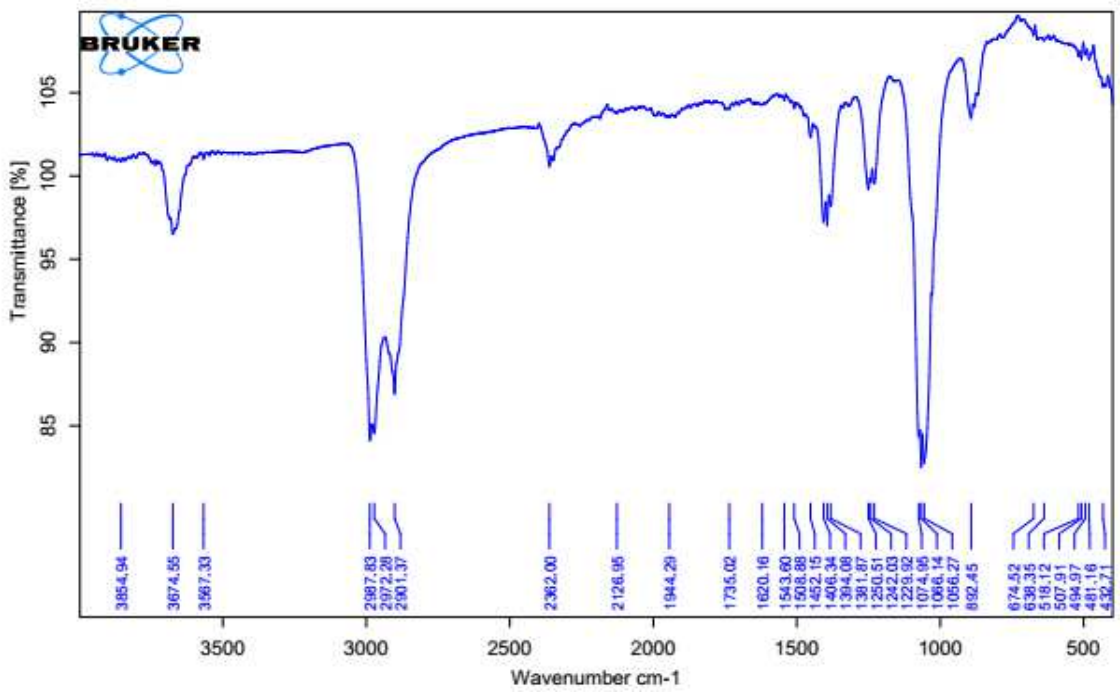


Fig 2: FTIR pattern of CA stalk fragments (After washing and drying)

Table 3: Functional groups obtained from FTIR [47]

Peak #	Wave number cm^{-1}	Group
1	3674.55	O-H Stretching
2	2987.83	N-H Stretching
3	2901.37	N-H Stretching
4	2362.00	C=O Stretching
5	1452.15	C-H Bending
6	1406.34	C-H Bending
7	1381.87	C-H Bending
8	1242.03	C-O Stretching
9	1066.14	C-O Stretching
10	1056.27	C-O Stretching
11	892.45	C=C Bending
12	674.52	C=C Bending

3.3 Calorific value

The gross calorific value of plant stalk fragments was measured at 14,990±90 $kJ.kg^{-1}$, showing its potential as an alternative fuel source [2].

3.4 Thermal analysis

Thermal analysis of CA stalks was carried out, as pointed out, at four heating rates in air, namely 5, 10, 15 and 20 K.min^{-1}, producing the corresponding EXCEL spreadsheets data from which TG – DTG curves obtained. Figure 2 represents the results at a heating rate of 5 K.min^{-1}.

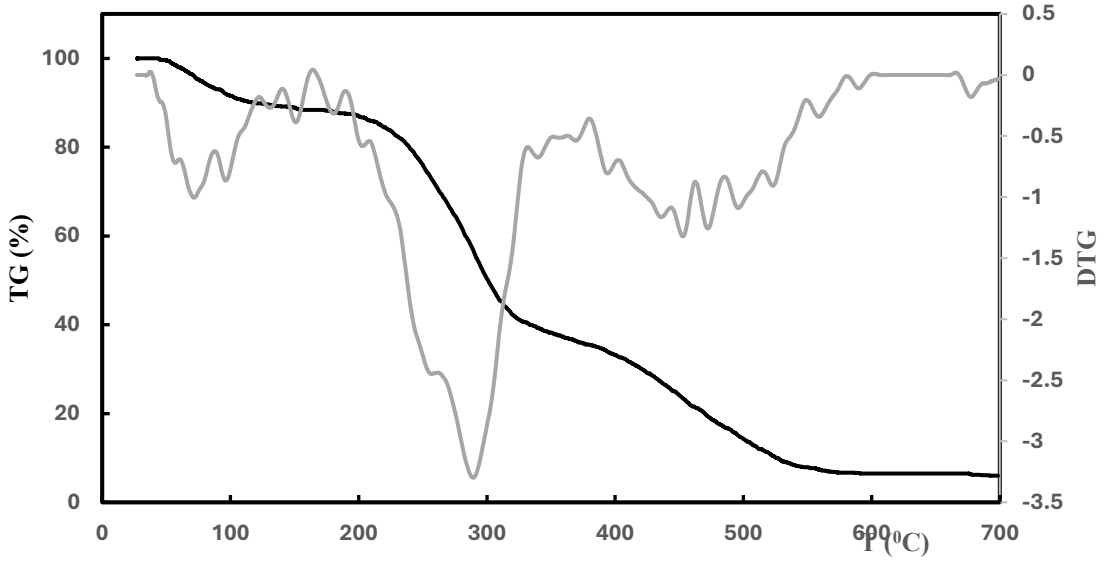


Fig 2: TG – DTG pattern for the thermal analysis of CA stalks at 5 K.min^{-1}

As can be observed from that figure, three peaks appear associated with a final weight loss of about 92% at 700°C, confirming the presence of about 9% ash, in close accordance with Table 2. The first peak, corresponding to a weight loss of about 9%, represents a loss of moisture. This value also fairly agrees with that reported in Table 2. The second peak, ending at about 384ºC corresponds to a mass loss of about 56%. Considering the results in Table 2, this figure agrees with that reported for the loss in mass due to the devolatilization of lignocellulosic components (55.69%). This step ends at about 580ºC, the exact temperature depending on the heating rate. Further heating causes devolatilization of volatile hydrocarbons, resulting in a decrease in the carbon content of the char residue, so that at 700ºC, there remains only 8.8% of the original material. This pattern has been reported for the thermal degradation of agricultural waste by many authors [48, 49].

3.5 Conversion curves for the first degradation step

These curves were drawn using the TG-DTG spreadsheets available at each heating rate and represent the relation between conversion and temperature for the first peak in Figure 2 with similar figures at other heating rates. Figure 3 displays this dependence. Third-degree polynomials could be fitted through the experimental points at the four rates with R^2 values > 0.999 in all cases. These functions allowed for the precise calculation of $\frac{d\alpha}{dT}$ whenever needed.

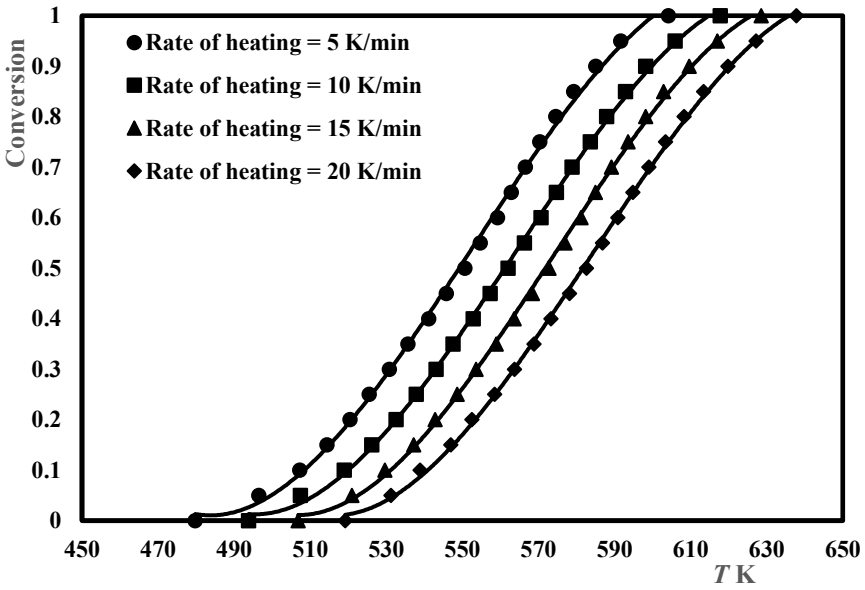


Fig 3: Conversion curves for the first step of degradation of CA stalks

3.6 Kinetic calculations for the first step of degradation

3.6.1 Coats – Redfern method

Values of $\ln \frac{g(\alpha)}{T^2}$ were calculated from conversion data at the four heating rates using all the kinetic functions $g(\alpha)$ reported in Table 1. The following results were obtained for average values of activation energy and the corresponding value of R^2 (Table 4).

Table 4: Values of average activation energy for different kinetic functions (First step of degradation)

Code	A2	A3	F1	F2	R2	R3	D2	D3	D4
β = 5K.min^{-1}									
E kJ.mol^{-1}	37.35	21.85	83.75	53.80	69.33	73.86	138.37	156.79	144.55
R^2	0.993	0.991	0.995	0.828	0.982	0.988	0.977	0.984	0.982
β = 10K.min^{-1}									
E kJ.mol^{-1}	38.45	22.51	86.17	55.78	71.25	75.94	142.10	161.15	148.49
R^2	0.992	0.990	0.994	0.842	0.979	0.986	0.974	0.983	0.979
β = 15K.min^{-1}									
E kJ.mol^{-1}	40.36	23.72	90.16	58.51	74.58	79.47	148.51	168.39	155.18
R^2	0.993	0.991	0.995	0.845	0.979	0.986	0.974	0.983	0.979
β = 20K.min^{-1}									
E Kj.mol^{-1}	41.58	24.48	92.77	60.25	76.75	81.78	152.73	173.17	159.59
R^2	0.994	0.992	0.995	0.847	0.980	0.987	0.974	0.982	0.980

This table reveals that the most probable mechanism is a first order reaction (F1) with an average value of activation energy = 88.21 kJ.mol^{-1}. The A2 and A3 mechanisms also produced high values of R^2. However, the crystallization and subsequent growth of crystals in the char phase remaining at the end of the step is not a likely possibility.

2.6.2 Criado's Normalized Master Plots

To test the viability of the second order reaction F2 mechanism, Criado's master plots were constructed using the Coats-Redfern at a heating rate of 10 K.min^{-1}. Figure 4 shows that the curve closest to experimental data is that of a first order reaction (F1).

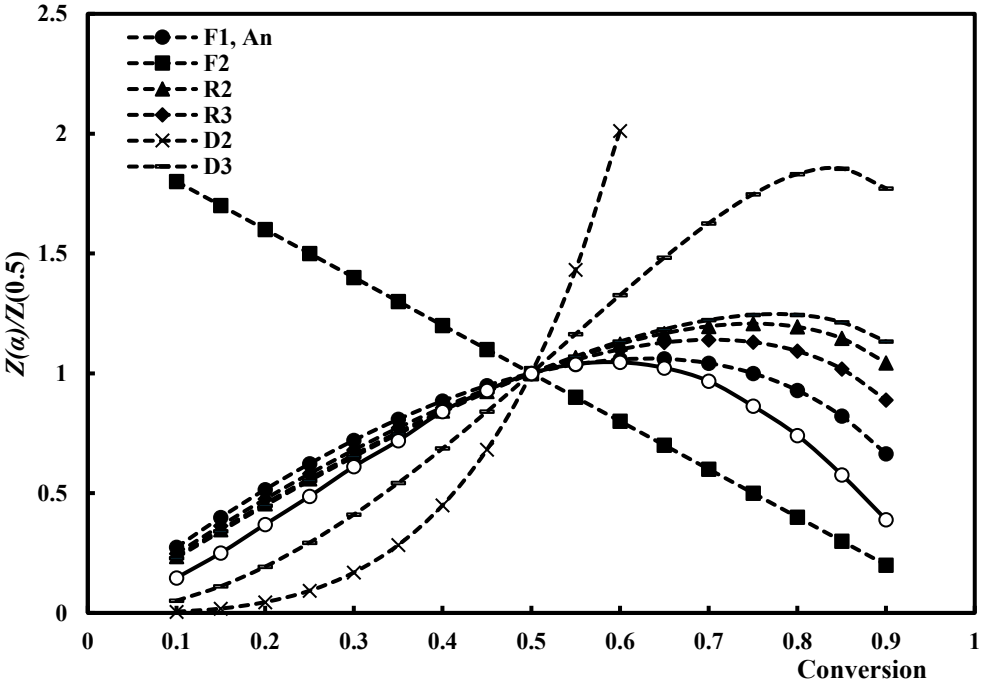


Fig 4: Criado's master plots for plots for the first degradation step of CA stalks

3.6.3 FWO method

The FWO plots, consisting of plotting $\log\beta$ against $1/T$ are presented in Figure 5 for conversion levels varying from 0.1 to 0.9. The slopes of the straight lines obtained were not equal, so that the values of activation energy showed an increase up to $\alpha = 0.7$, then remained almost constant (Table 5). The average value of E was determined to be 107.62 kJ.mol^{-1}.

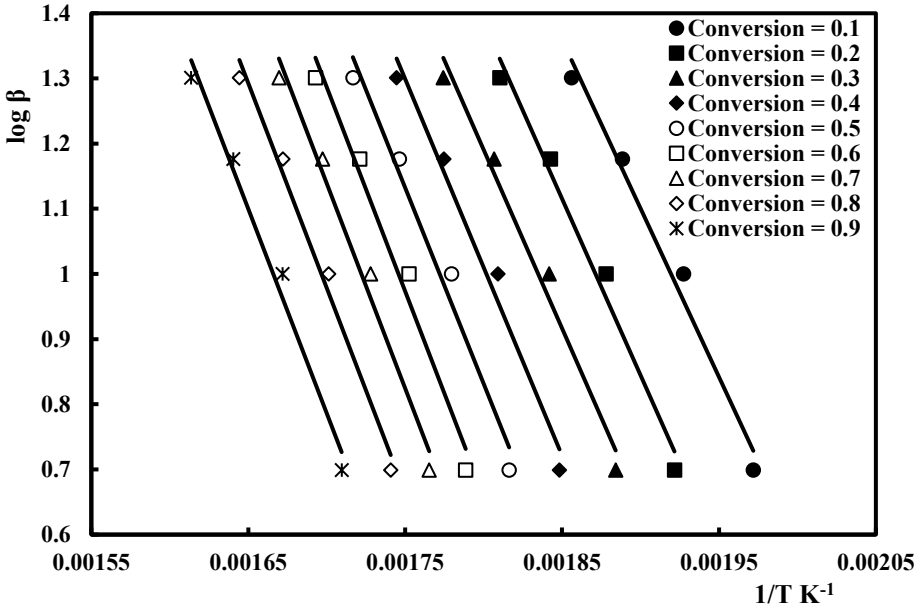


Fig 5: FWO plots for the first degradation step of CA stalks

3.6.4 KAS method

The straight lines obtained on plotting $\ln\frac{\beta}{T^2}$ against $1/T$ produced the straight lines displayed in Figure 6. Here also, activation energy values tended to increase up to $\alpha = 0.7$ before steadying. (Table 5). The average value of E was almost equal to that determined by the FWO method, as it equals 103.88 kJ.mol^{-1}.

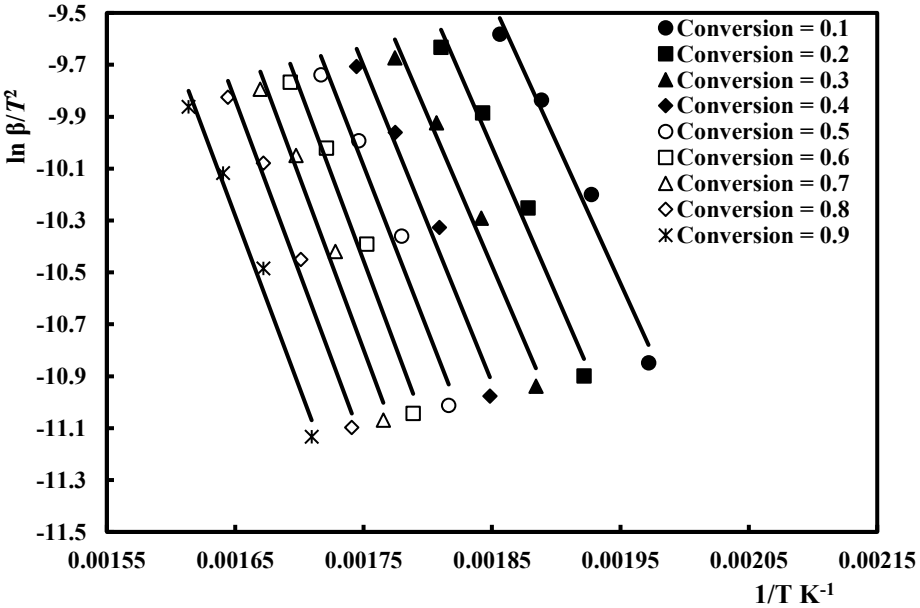


Fig 6: KAS plots for the first degradation step of CA stalks

3.6.5 Friedman method

This method requires determining the values of $\ln \beta . \frac{d\alpha}{dT}$ at each conversion level, which was carried out by obtaining the equations of the third-degree polynomials in the form $\alpha = \alpha(T)$ and differentiating these equations to obtain accurate values for $\frac{d\alpha}{dT}$. For example, the equation of the regression curve obtained at a heating rate of 10°C.min^{-1} is:

$\alpha = -8.1786 \times 10^{-7} T^3 + 0.001383 T^2 - 0.7682 T + 140.592$

Which, upon differentiation yields:

$\frac{d\alpha}{dT} = -2.4536 \times 10^{-6} T^2 + 0.002766 T - 0.7682$

The Friedman plots of $\ln \beta . \frac{d\alpha}{dT}$ against $1/T$ are presented in Figure 7. The variation of activation energy with conversion almost follows the same trend observed in the two previous techniques, although its values tended to slightly decrease as conversion approached unity. (Table 5). The average value of E equals 112.31 kJ.mol^{-1}, somewhat higher than the two previous results.

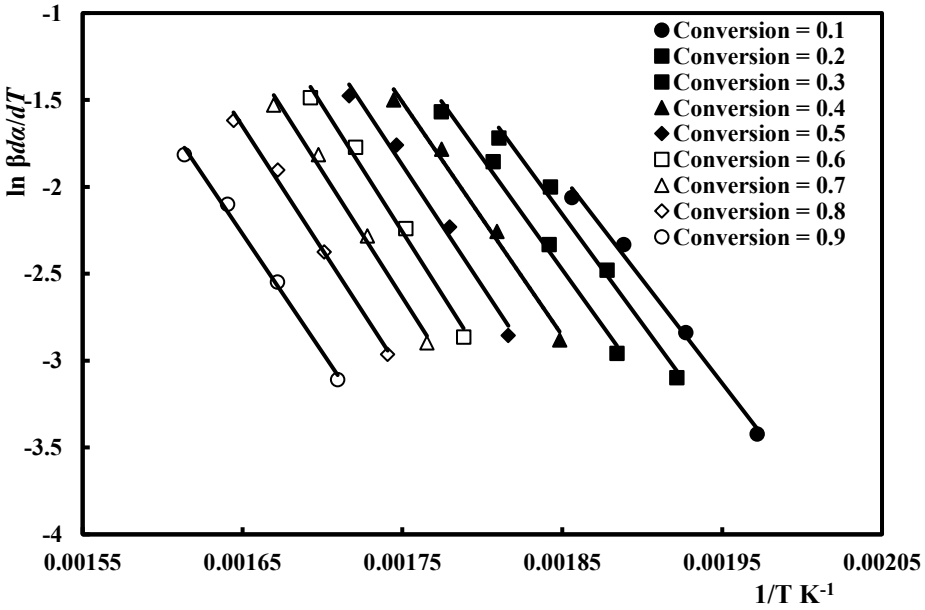


Fig 7: Friedman plots for the first degradation step of CA stalks

Table 5: Variation of activation energy with conversion in iso-conversional methods. For the first degradation step (kJ.mol^{-1})

α	0.1	0.2	0.3	0.4	0.5	0.6	0.7	0.8	0.9	Mean
FWO	94.22	98.55	99.86	109.23	109.45	114.10	114.53	114.42	114.19	**107.62**
KAS	90.39	94.72	95.92	106.40	105.68	110.43	110.76	110.50	110.08	**103.88**
Friedman	99.31	104.55	106.60	111.74	115.97	120.65	120.30	118.17	113.50	**112.31**

As can be noticed from Table 5, the average values of activation energy determined by the three iso-conversional methods are comparable. The reasons for the discrepancy observed in the mean values of activation energy obtained using the model technique of Coats – Redfern and those obtained by iso-conversional methods can be attributed to the following reason: The presence of overlapping reactions, typical of decomposition of lignocellulosic components, cannot always be explained by assuming a simple kinetic mechanism like F1 in the present case. This way, the value of activation energy determined at any heating rate will not necessarily indicate its true value [50]

3.6.6 Determination of the relation between ln A and activation energy

The determination of the logarithm of the pre-exponential factor was carried out by the method suggested by Vyazovkin et al [46] and outlined in section 2.2. The average values of activation energy obtained by the Coats-Redfern method at each heating rate and reported in Table 4 were used along with the values of $\frac{d\alpha}{dt} = \beta.\frac{d\alpha}{dT}$ to determine the values of $\ln A$ for all types of kinetic functions $f(\alpha)$. Figure 8 shows the results obtained on plotting the different values of $\ln A$ against corresponding values of E at the four heating rates investigated. The points align on a straight line of equation:

$\ln A = -2.9179 + 0.2171E$ $\quad R^2 = 0.995$

Using this equation, it was possible to assign values of $\ln A$ to correspond to average activation energy values obtained by iso-conversional methods. The following table summarizes the results.

Table 6: Average values of activation energy and ln A for the first degradation step

Method	**FWO**	**KAS**	**Friedman**
E kJ.mol^{-1}	107.62	103.88	112.31
ln A	20.45	19.63	21.46

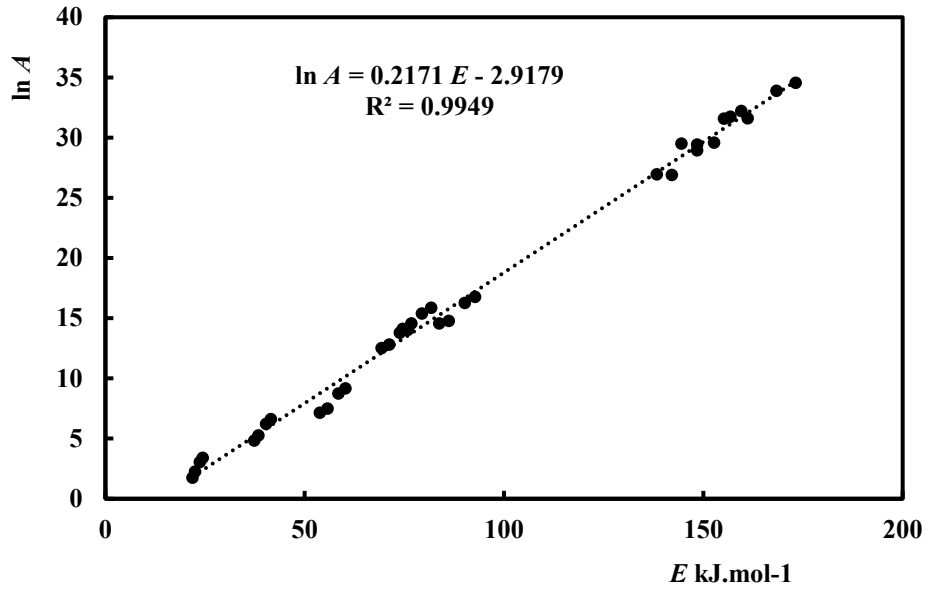


Fig 8: Plots of ln*A* against *E* for the first degradation step

3.7 Conversion curves for the second degradation step

Figure 9 shows the experimental conversion curves. Third-degree polynomials modelled the four curves with a minimum R^2 value = 0.9992.

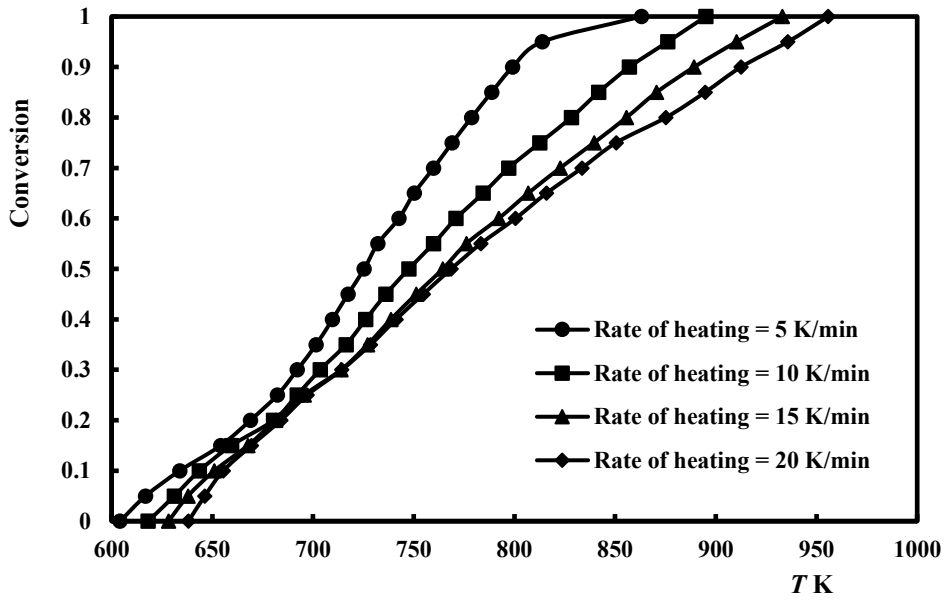


Fig 9: Conversion curves for the second step of degradation of CA stalks

3.8 Kinetic calculations for the second step of degradation

The same kinetic analyses used for the first stalk-degradation step were applied to the second step, omitting redundant figures for brevity.

3.8.1 Coats – Redfern method

Plots of $\ln \frac{g(\alpha)}{T^2}$ against $1/T$ were performed from conversion data at the four heating rates using all the kinetic functions $g(\alpha)$ reported in Table 1. Table 7 summarizes the results.

Table 7: Values of average activation energy for different kinetic functions (second step of degradation)

Code	A2	A3	F1	F2	R2	R3	D2	D3	D4
β = 5 K.min^{-1}									
E kJ.mol^{-1}	27.38	14.27	66.63	40.70	54.56	58.36	113.18	128.58	118.35
R^2	0.999	0.997	0.999	0.779	0.990	0.995	0.980	0.986	0.981
β = 10 K.min^{-1}									
E kJ.mol^{-1}	19.46	8.84	51.26	31.29	41.26	44.40	88.39	101.15	92.66
R^2	0.980	0.950	0.990	0.813	0.964	0.975	0.963	0.982	0.971
β = 15 K.min^{-1}									
E kJ.mol^{-1}	16.50	6.78	45.61	27.43	36.43	39.32	79.53	91.25	83.46
R^2	0.966	0.903	0.984	0.803	0.954	0.967	0.956	0.977	0.964
β = 20 K.min^{-1}									
E Kj.mol^{-1}	14.55	5.42	41.90	25.37	33.15	35.90	73.45	84.59	77.18
R^2	0.932	0.791	0.970	0.830	0.928	0.945	0.936	0.962	0.946

This table reveals the strong dependence of the values of activation energy on heating rate. The values of R^2 designate a first order F1 mechanism as the most probable mechanism. The average value of E = 51.35 kJ.mol^{-1}.

3.8.2 Criado's Master Plots

Figure 10 represents the Master Plots determined from data at 10 K.min^{-1}. This figure shows that, while the curve corresponding to a first order reaction (F1) is consistent with experimental results for up to 0.55 conversion, a second order mechanism seems to be favored at higher conversion levels. This is typical of the devaporization of solid matter at higher temperatures in the degradation of agricultural waste where a shift in the reaction mechanism is a common occurrence [51].

3.7.3 FWO method

FWO plots revealed a steady decrease in activation energy following increasing conversion from a value of 208.32 kJ.mol^{-1} at $\alpha = 0.1$ to 70.09 kJ.mol^{-1} at $= 0.9$, with an average value of 144.15 kJ.mol^{-1}. (Table 8)

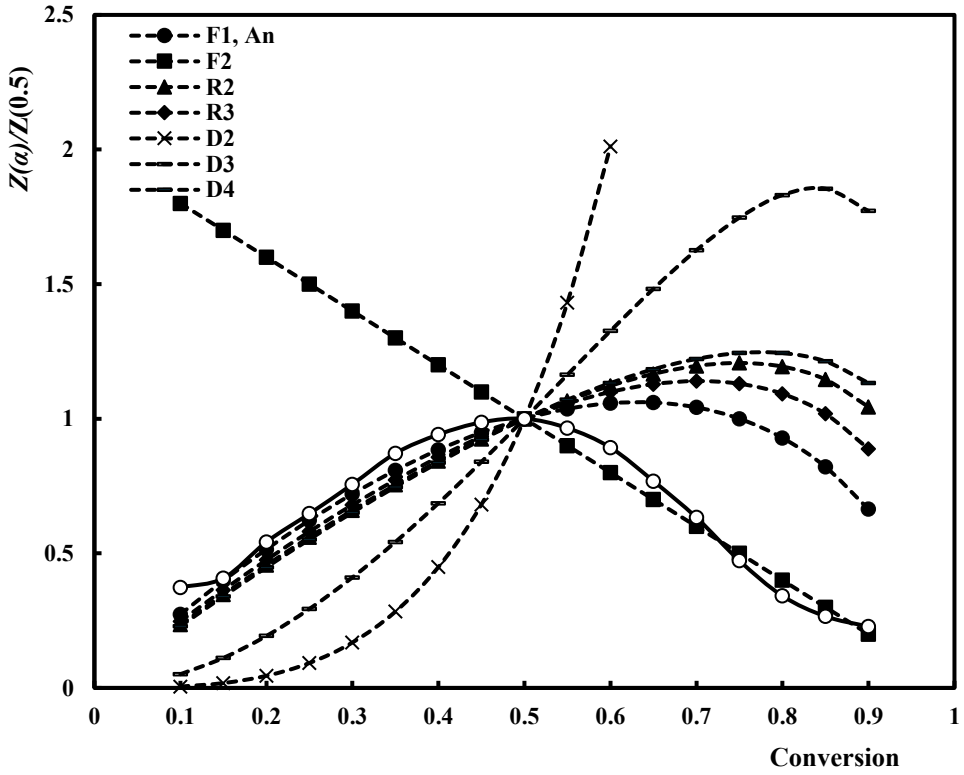


Fig 10: Criado's master plots for plots for the second degradation step of CA stalks

3.7.4 KAS method

The KAS results were compatible with those of FWO since the values of E steadily decreased from 208.36 kJ.mol^{-1} at $\alpha = 0.1$ to 59.56 kJ.mol^{-1} at $= 0.9$, averaging 139.81 kJ.mol^{-1}. (Table 8)

3.7.5 Friedman method

Likewise, the results obtained from Friedman's plots showed the same decrease in activation energy values from 330.53 kJ.mol^{-1} at $\alpha = 0.1$ to 50.38 kJ.mol^{-1} at $= 0.9$, averaging 133.75 kJ.mol^{-1}. (Table 8)

It appears that the average value of E obtained by the three non-model methods are close and considerably higher than that obtained using the Coats-Redfern model technique.

Table 8: Variation of activation energy with conversion in iso-conversional methods. For the second degradation step (kJ.mol^{-1})

α	0.1	0.2	0.3	0.4	0.5	0.6	0.7	0.8	0.9	Mean
FWO	208.32	210.95	221.04	175.53	134.06	108.95	91.47	76.94	70.09	**144.15**
KAS	208.35	215.76	220.75	173.32	128.57	101.76	82.98	67.22	59.56	**139.81**
Friedman	330.53	319.06	172.93	110.68	75.00	55.61	46.53	43.10	50.38	**133.76**

3.7.6 Determination of the relation between ln *A* and activation energy

The same procedure adopted for the first degradation step was used here. The straight line associated with the kinetic compensation mechanism is presented in Figure 11 and its characteristic equation is:

$\ln A = -3.55 + 0.1768E$ $R^2 = 0.947$

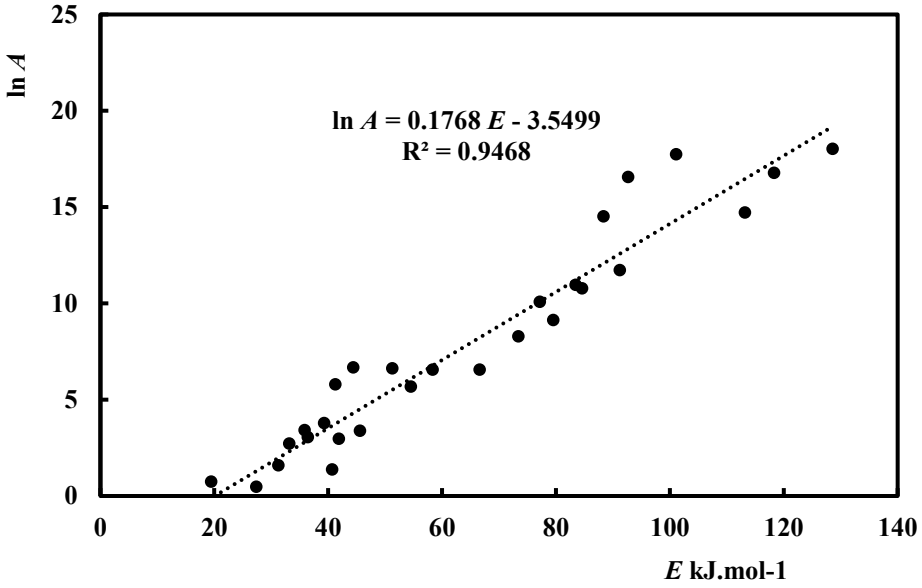


Fig 11: Plots of ln*A* against *E* for the second degradation step

Consequently, values of ln *A* can be computed from the average values of activation energy obtained by the three iso-conversional techniques. The results are summarized in Table 8.

Table 8: Average values of activation energy and ln *A* for the second degradation step

Method	FWO	KAS	Friedman
E kJ.mol^{-1}	144.15	139.81	133.76
ln *A*	21.9439.81	21.17	20.10

4. Sustainability issues in using the present waste as alternative fuel

In that respect, two issues are considered, regarding the partial or total substitution of CA stalks for charcoal, currently used as major fuel in Egyptian industry.

First, the effect of substituting fossil fuels by the present waste on CO_2 emissions produced from burning is considered. In the event of total substitution, the use of such waste will cause a moderate decrease in emissions. On one hand, the carbon content of the waste is

40.6% (Table 2) and consequently, 1 kg waste will produce $\frac{0.406\times44}{12}$ = 1.49 kg CO_2. Since the calorific value of the waste = 14990 kJ.kg^{-1}, then its CO_2 equivalent is about 10^{-4} kg CO_2 per kJ. On the other hand, if charcoal is used as fossil fuel its CO_2 equivalent is about 1.3×10^{-4} kJ.kg^{-1} [52]. Therefore, upon full substitution of fossil fuel, CO_2 emissions will decrease by about 23%.

The second factor is of economic nature. The fixed cost of agricultural stalks is negligible compared to that of charcoal, especially when charcoal must be imported, as is the case in Egypt.

Regarding operating expenses, the cost of processing stalks for a boiler or furnace burner primarily involves drying and attrition (typically in a pan mill). Because charcoal lumps require the same drying and grinding processes, these baseline operations incur comparable costs.

Consequently, while stalks offer a clear advantage in fixed costs, completely or partly substituting charcoal with stalks will not practically affect the operating cost.

However, totally substituting fossil fuel by the present waste is subject to some restrictions. First, the ash content of high-quality charcoal is lower than that of stalks of CA [53] (1 – 4% compared to 9 – 10%). Also, transporting bulky agricultural stalks hinders the delivery of sufficient quantities for combustion. To resolve this, the waste is often compressed into small briquettes for easier transportation. However, this method requires shredding the briquettes back down at the factory site before use.

In conclusion, while the use of CA stalks provides a means of lowering CO_2 emissions, there is a need for further study to assess the most economical range of their substitution for conventional fossil fuels such as charcoal, whether in boilers or industrial kilns burners.

5. Conclusions

Stalks of a noxious herbaceous biomass, *Chenopodium album* have been considered for possible use as alternative fuel in boilers or furnace burners. Proximate analysis proved that their carbon content = 40.6.% and their lignocellulosic compounds contents were obtained: Hemicellulose = 9.44%, cellulose = 34.26% and lignin = 11.99%. Also, the calorific value was evaluated at 14990 kJ.kg^{-1}.

Thermal analysis in air was carried out at four heating rates, namely, 5, 10, 15 and 20 K.min^{-1}, where two DTG peaks appeared ending about 600^{o}C, leaving about 9% ash residue. The kinetics of the two steps of degradation were studied using two model fitting methods: The Coats-Redfern and Criado's master plots methods and three iso-conversional techniques, FWO, KAS and Friedman methods.

The first degradation step proved to be controlled by a first order (F1) mechanism and the average activation energy values obtained by the FWO, KAS and Friedman techniques were very close (107.62, 103.88 and 112.31 $kJ.mol^{-1}$, respectively). The values of ln *A* were consequently determined using the kinetic compensation principle, yielding the respective values 20.45, 19.63 and 21.46 (*A* in min^{-1}).

The second degradation step proved to be more complex, since Criado's master plots showed a shift from F1 to F2 mechanism as conversion increased. The average values of activation energy predicted by the three iso-conversional methods were close ranging from 133.76 to 141.15 $kJ.mol^{-1}$, with corresponding values of ln *A* ranging from 17.85 to 19.48.

The effect of substituting charcoal, as fossil fuel, by *Chenopodium album* stalks on CO_2 release proved that total substitution resulted in 23% decrease in emissions, while from an economic standpoint, replacing the material with stalks lowers fixed costs without much affecting operating expenses. For use in any industry, the extent of substitution is regulated by the necessary heat load and the nature and amount of ash produced on burning.

6. Data availability

All data generated or used during this study are included in this published article and its supplementary information files.

7. References

[1] Abdel Halim, N.Y., Muhammad, N.I.S., Mansur, F.Z., Ahmad, N. (2025) "Sustainable fuel from agricultural waste: Mixture design optimization of refuse-derived fuel for enhanced energy output" Next sustain. 6: 100196. http:// doi.org/10.1016/j.nxsust.2025.100196

[2] Setiawan, A., Nugraha, A., Cahyono, L, Nindyapuspa, A., Widiana, D.R., Kusuma, S.A. (2025) "The Study on utilization of agricultural waste as an alternative fuel for bio-briquettes" Int. J. Progress. Sci. Tech. 40(1):44. DOI:10.52155/ijpsat.v40.1.5540

[3] Psomopoulos, C.S., Themelis, N.J. (2014) "Use of alternative fuels in cement industry" 12th Int. Conf. on Protection and Restoration of the Environment, Skiathos island, Greece, 1: 521-529.

[4] Metwally, E.M., Zahran, A.A., Fattah, M.K. (2024) "Uses of alternative fuels in cement industrial sectors as sustainable development option" Int. J. Environ. Studies Res. 3(2): 66–73

[5] Kepplinger, W.L., Tappeiner, T. (2012) "Solid recovered fuels in the steel industry" Waste Manag. Res. 30(4): 450–453. DOI: 10.1177/0734242X11426174

[6] Taj, W., Qayum, A., Algarni, F., Malik, F., Jan, S.U. (2025) “Evaluating the use of alternative fuels in cement production for environmental sustainability” Sustainability, 17(13): 5924. https://doi.org/10.3390/su17135924

[7] Nour, M., Amer, M. Elwardany, A., Attia, A., Li, X., Nada, S. (2021) “Pyrolysis, kinetics, and structural analyses of agricultural residues in Egypt: For future assessment of their energy potential” Clean. Eng. Tech. 2: 100080. https://doi.org/10.1016/j.clet.2021.100080

[8] Maiti, D., Kundu, P., Adhikari, S. (2026) “Bioreactor design guided by kinetic modeling: a sustainable approach” Braz. Arch. Bio. Tech. 69: e26250869. https://doi.org/10.1590/1678-4324-2026250689

[9] Perez-Velasquez, M.A., Santes, V., Balmaseda, J., Torres-Gracia, E. (2013) “Pyrolysis of orange waste: A thermo-kinetic study”. J. Anal. Appl. Pyrolysis 99: 170–177. http://dx.doi.org/10.1016/j.jaap.2012.09.016

[10] Chilla, V., Suranani, S. (2023) “Thermogravimetric and kinetic analysis of orange peel using iso-conversional methods” Mater. Today Proc. 72(1): 104–109. https://doi.org/10.1016/j.matpr.2022.06.196

[11] Mousa, S., Dubdub, E., Al Faiad. M.A., Younes, M.Y., Ismail, M.A. (2025) “Characterization and kinetic study of agricultural biomass orange peel waste combustion using TGA Data” Polymers 17(8), 1113. https://doi.org/10.3390/polym17081113

[12] Muhammad, F., Nisar, J., Ali, G., Anwar, F., Ghani, W.W., Sharif, A., Ahmed E. (2023) “Pyrolysis of sweet lemon (Citrus limetta) waste” Energy Adv. 4(3): 414–423. https://doi.org/10.1039/d4ya00600c.

[13] Ismail, M.A., Dubdub, E., S. Mousa, Al Yaari, M., Al Faiad, M.A., Alshehab, A. (2025) Assessing lemon peel waste as a solid biofuel: A Study of its combustion behavior, Kinetics, and Thermodynamics” Polymers 2025, 17(21), 2830. https://doi.org/10.3390/polym17212830.

[14] Dubey, S., Kumar, R., KumarMondal, M. (2022) “Pyrolysis kinetics and thermodynamics of pomegranate peel using TG/DTG analysis” Biomass Conv. Refin. 14(11):1–15. DOI:10.1007/s13399-022-03288-1

[15] Zaman, F., Du, Z., Munawar, A., Ishaq, M.W., Guan, Y. (2023) “Pyrolysis kinetics and conversion of pomegranate peels into porous carbon” Environ. Prog. Sust. Energy. 42(5): e14153. https://doi.org/10.1002/ep.14153

[16] Kumar, S.A.P., Nagarajan, R., Prasad, K.M., Anand, B., Murugavelh, S. (2022) "Thermogravimetric study and kinetics of banana peel pyrolysis: a comparison of 'model-free' methods" Biofuels 13(2): 129–138. https://doi.org/10.1080/17597269.2019.1647375

[17] Felobes, R.A., Abadir, M.F. (2024) "Modeling the kinetics of pyrolysis of date seeds using artificial neural networks" Renew. Energy Sust. Develop. 10(1): 123–134. http://dx.doi.org/10.21622/RESD.2024.10.1.811

[18] Xie, H., Yu, Q, Duan, W., Wang, K., Li, X., Shi, X. (2013) "Pyrolysis characteristics and kinetics of lignin derived from three agricultural wastes" J. Renew. Sust. Energy 5: 063119. https://doi.org/10.1063/1.4841215

[19] Shi, X., Zhou, X., Chen, W., Wang X., Nguyen, T., Chen N. (2017) "Thermal and kinetic behavior of fallen leaves and waste tires using thermogravimetric analysis" BioRes. 12(3): 4707–4721. DOI:10.15376/biores.12.3.4707-4721

[20] Melikoglu, M., Ozdemir, M. Ates, M. (2023) "Pyrolysis kinetics, physicochemical characteristics and thermal decomposition behavior of agricultural wastes using thermogravimetric analysis" Energy nexus, 11: 100231. https://doi.org/10.1016/j.nexus.2023.100231.

[21] Llaymia, I., Belaadi, A., Gernaout, D. (2025) "Studying Gaussian deconvolution and multicomponent kinetics models in Agave cellulosic fibers pyrolysis: Application in sustainable bioenergy for cleaner production" Biomass Bioenergy, 192: 107488. https://doi.org/10.1016/j.biombioe.2024.107488.

[22] Abdel Raouf, J., Abdelhady, H.M., Abadir, M.F., Sibak, H.A. (2022) "Kinetics of pyrolysis of water hyacinth: A novel empirical approach" Egypt. J. Chem. 45(12): 467–479. DOI:10.21608/ejchem.2022.125143.5565

[23] Aly, S.T., Mahmoud, F. El-Z., Sorour, M.A., Abadir, M.F., El Saidy, M.I. "Kinetics of pyrolysis of de-oiled neem seeds (*Azadirachta indica*)". Biomass Conv. Refin. 15(5):7809–7826. DOI :10.1007/s13399-024-05677-0

[24] Biagini, E., Barontini, F., Tognotti, L. (2016) "Thermal decomposition of agricultural and food residues: Comparison of kinetic models" Can. J. Chem. Eng. 95(5): DOI:10.1002/cjce.22738

[25] Cano-Pleite, E., Rubio-Rubio, M., Riedel, U., Soria-Verdugo, A. (2021) "Evaluation of the number of first-order reactions required to accurately model biomass pyrolysis" Chem. Eng J. 408: 127291. https://doi.org/10.1016/j.cej.2020.127291

[26] Ozmen, O., Mor, F. (2003) "Nitrate poisoning in cattle fed Chenopodium album hay" Vet. Human. Toxic. 45(2): 83–84.

[27] Demiray, A., Yilmaz, T., Demiray, S., Akgùn, H., Koçyiğit, I. (2024) “A case of acute tubulointerstitial nephritis following the use of *Chenopodium album* L” Int. J. Emergency Med. 17:189. https://doi.org/10.1186/s12245-024-00790-3

[28] Holm, LeRoy G., Plucknett, Donald L., Pancho, Juan V.; Herberger, James P. (1977). “The World's Worst Weeds: distribution and biology”. Honolulu: University Press of Hawaii. p. 84

[29] Batish, D., Singh, H.P., Rana, N., Kohli, R. (2006) “Assessment of allelopathic interference of *Chenopodium album* through its leachates, debris extracts, rhizosphere and amended soil” 52(6): 705–715. DOI:10.1080/03650340601037119

[30] Mohamed, I.A. (2023) “The potency of separated and new premix formulations of carfentrazone- based herbicide against annual broadleaved weeds in wheat” Egypt. Acad. J. Biology. Sci., 15(1):35-45.

[31] Ramos-Pacheco, B.S., Ligarda-Samanez, C.A., Choque-Quispe, D., Choque-Quispe, Y., Solano-Reinozo, A.M., Choque-Quispe, K. Palomino-Rincón, H., Taipe-Pardo, F., Peralta-Guevara, D.E., Moscoso-Moscoso, E. (2025) “Study of the physical–chemical, thermal, structural, and rheological properties of four high Andean varieties of germinated *Chenopodium quinoa*” Polymers 17(3): 312. https://doi.org/10.3390/polym17030312

[32] F. Salama, M. Abd El-Ghani, N. El-Tayeh, A. Amro, and H. Abdrabbu, “Weed flora of common crops in desert reclaimed arable lands of southern Egypt,” *Taeckholmia*, vol. 36, no. 1, pp. 58–76, 2016, doi: 10.21608/taec.2016.11940.

[33] A. Gaafar, “Morphology and Stem Anatomy of Chenopodium Species from Egyptian Flora,” *Egypt. J. Bot.*, vol. 59, no. 1, pp. 53–58, 2019, doi: 10.21608/ejbo.2018.4699.1193.

[34] Dampanaboina, L., Yuan, N., Mendu. V. (2021) “Estimation of crystalline cellulose content of plant biomass using the Updegraff Method” J. Vis. Exp. 15(171): DOI: 10.3791/62031

[35] Sura-Kalixto, F., Canellas, J., Barrio, A., Garcia-Razo, G. (2020) “Determination of hemicellulose, cellulose, and lignin content in different types of biomasses” Processes 8(9): 1048; https://doi.org/10.3390/pr8091048

[36] ASTM E1756 (2020) “Standard Test Method for Determination of Total Solids in Biomass”

[37] ASTM E1755 (2020) “Standard Test Method for Ash in Biomass”

[38] ASTM E872 (2020) “Volatile Matter Testing in Biomass”

[39] Khawam, A., Flanagan, D. R. (2006). “Solid-state kinetic models: Basics and mathematical fundamentals”. J. Phys. Chem. B, 110 (35): 17315–17328. https://doi.org/10.1021/jp062746a

[40] Monir, M.U., Shovon, S.M., Akash, S.A., Habib, M.A., Teshata, K., Aziz, A.A., Chowdhury, S., Prasetya, T.A.E. (2024) “Comprehensive characterization and kinetic analysis of coconut shell thermal degradation: Energy potential evaluated via the Coats-Redfern method” Case Studies Therm. Eng. 55: 104186. https://doi.org/10.1016/j.csite.2024.104186

[41] Otaru, A., Zaid, A.A.A. (2025) “Thermal degradation of palm fronds/polypropylene bio-composites: thermo-kinetics and convolutional-deep neural networks techniques” Polymers, 17(9): 1244. DOI:10.3390/polym17091244

[42] Wanjun, T., Liu, Y., Xil, Y., ZhiYong, W. (2005) “Approximate formulae for calculation of the integral $\int \exp(-E / RT).dT$” J. Therm. Anal. Calorimetry 81(2): 347–349. DOI:10.1007/s10973-005-0790-7

[43] Sirinwaranon, P., Atong, D., Sricharoenchaikul, V. (2019) “Thermal degradation and kinetic study of Cassava Rhizome for torrefaction application”. IOP Conf. Series: Earth Environ. Sci. 401: 012007. DOI:10.1088/1755-1315/401/1/012007

[44] Matali, S., Rahman, N.A., Idris, S.S., Yaacoub, N. (2020) “Dynamic model-free and model-fitting kinetic analysis during torrefaction of oil palm frond pellets” Bull. Che. Reaction Eng. Cat. 15(1): 253–263 DOI:10.9767/bcrec.15.1.6985.253-263

[45] Fedunik-Hofman, L., Bayan, A., HinklEy, J., Lipiński, W., Donne, S.W. (2019) “Friedman method kinetic analysis of CaO-based sorbent for high-temperature thermochemical energy storage” Chem. Eng. Sci. 200: 236–247. https://doi.org/10.1016/j.ces.2019.02.003

[46] Vyazovkin, S., Burnham, A. K., Criado, J. M., Pérez-Maqueda, L. A., Popescu, C., Sbirrazzuoli, N. (2018). “ICTAC Kinetics Committee recommendations for performing kinetic computations on thermal analysis data”. Thermochimica Acta, 673, 1–7. https://doi.org/10.1016/j.tca.2018.01.002

[47] https://instanano.com/all/characterization/ftir/ftir-functional-group-search/

[48] Tamo, A.K., Doench, I., Deffo, G., Jiokeng, S.F.Z., Doungmo, G., Fotsop, C.G., Temgoua, R.C.T., Montembault, A., Serghei, A., Njanja, E., Tonle, I.K., Osorio-Madarzo, A. (2025) “Lignocellulosic biomass and its main structural polymers as

sustainable materials for (bio)sensing applications" J. Mater. Chem. A 13: 24185-24253. DOI: 10.1039/D5TA02900G

[49] J.A. Titiloye, M.S. Abu Bakar, T.E. Odetoye (2013) "Thermochemical characterization of agricultural wastes from West Africa" Ind. Crops Prod. 47, 199–203. https://doi.org/10.1016/j.indcrop.2013.03.011

[50] Khawam, A., Flanagan, D. R. (2005). "Role of iso-conversional methods in varying activation energies of solid-state kinetics: II. Non-isothermal kinetic studies" Thermichim. Acta 436(1-2): 101–112. http://doi.org/ 10.1016/j.tca.2005.05.015

[51] Nath, B., Chen, G., Bowtell, L., graham, E. (2023) "Kinetic mechanism of wheat straw pellets combustion process with a thermogravimetric analyzer" Heliyon 9(10: e20602. DOI:10.1016/j.heliyon.2023.e20602

[52] Nganko, J.M., Koffi, E.P.M., Toure, A.O., Tiogue, C.T., Ndiaye, B., Ba, K., Yao, K.B. (2025) " Comparative assessment of pollutant emissions between biofuel briquettes and charcoal: implications for domestic cooking fuel selection" Carbon Res. 4, 15. https://doi.org/10.1007/s44246-024-00177-2

[53] https://thecharcoalfactory.com/blog/charcoal-ash-content-moisture-specs/

Funding

The authors received no specific funding for this work.

Supplementary Files

This is a list of supplementary files associated with this preprint. Click to download.

- CHENATMBiomassConversion.xlsx
- Compensationeffectformatfirststep.xlsx
- Compensationeffectformatsecondstep.xlsx
- ChenAlbStalkTGA.xlsx
- ChenAlbumStalksAtmTGADTG.docx
- CHENFATMwithDTG.xlsx
- CalculationsofStalksCombustioninAir.xlsx
- STC.pdf